Volume 4 Issue 2 (September 2024)
DOI 10.24191/jaeds.v4i2.84
eISSN 2805-5756

Journal of Applied Engineering Design & Simulation

CFD Analysis of 500W Centrifugal Compressor Performance

M.Z. Azmizam[1], A.M.I Mamat[1,2,*]
[1]Smart Manufacturing Research Institute, Universiti Teknologi MARA, Shah Alam 40450 Selangor, Malaysia.
[2]School of Engineering, Universiti Teknologi MARA, Shah Alam 40450 Selangor, Malaysia.
[*]corresponding author: amanihsan@uitm.edu.my

ABSTRACT

This paper used Computational Fluid Dynamics (CFD) to analyse the performance of a 500W centrifugal compressor, aiming to develop a comprehensive performance map under various operating conditions. The methodology includes stages such as geometry and grid generation, mesh generation, boundary condition setup, and CFD analysis using ANSYS software. The compressor blade profile was generated using ANSYS BladeGen, followed by meshing that consists of roughly 446,886 nodes and 417,312 elements via ANSYS TurboGrid. Boundary conditions were established by using the CFX-Pre, detailing the inlet and outlet conditions, such as mass flow rate, total temperature, and total pressure. The CFD simulations were conducted using CFX-Solver for 500 iterations, targeting a residual mean square (RMS) of 1 × 10-5, and the results were analysed using CFX-Post. The analysis was conducted under ambient conditions with a mass flow rate ranging from 0.01 kg/s to 0.065 kg/s and speeds of 60,000 rpm, 70,000 rpm, and 80,000 rpm. The expected outcomes include detailed performance maps that provide valuable insights into parameters like Mass Flow Parameter (MFP), Pressure Ratio (PR), and Efficiency (η) across different operating conditions. By employing the k-ε turbulence model in ANSYS CFX, the project aims to offer significant insights into the compressor's performance characteristics. The analysis, conducted under ambient conditions with a mass flow rate ranging from 0.01 kg/s to 0.065 kg/s and speeds of 60,000 rpm, 70,000 rpm, and 80,000 rpm, yielded significant results. The maximum power achieved at the design speed was 771 W at a mass flow rate of 0.05 kg/s. The maximum efficiency recorded was 77.8% at the same mass flow rate, with the efficiency average around 65.5% across the design speed.

Keywords: *Turbomachinery, centrifugal compressor, ANSYS TurboGrid, performance map, k-ε turbulence mode;*

Nomenclature (Greek symbols towards the end)

A_1	Area Inlet (m^2)
A_2	Area Outlet (m^2)
b_2	Outlet Length (m)
C_1	Inlet Absolute Velocity (m/s)
C_2	Outlet Absolute Velocity (m/s)
C_{a1}	Inlet Axial Velocity (m/s)
C_{m2}	Outlet Meridional Velocity (m/s)
$C_{\theta 1}$	Inlet Tangential Velocity (m/s)
$C_{\theta 2}$	Outlet Tangential Velocity (m/s)
C_p	Specific Heat at Constant Pressure (kJ/kg°C)
C_v	Specific Heat at Constant Volume (kJ/kg°C)
h	Enthalpy (J/kg)
$\dot{m}$	Mass Flow Rate (kg/s)
N	Rotational Speed (rpm)
P_0	Stagnation Pressure (Pa)
P_{is}	Isentropic Pressure (Pa)
P_{ref}	Reference Pressure (Pa)
$\dot{Q}_{corr}$	Corrected Mass Flow Rate (kg/s)
T_{ref}	Reference Temperature (K)
U_1	Inlet Blade Speed (m/s)
U_2	Outlet Blade Velocity (m/s)
W_1	Inlet Relative Velocity (m/s)
W_2	Outlet Relative Velocity (m/s)
$\dot{W}_{C,a}$	Actual Power (W)
$\dot{W}_{C,is}$	Isentropic Power (W)
α	Absolute Angle, °
β	Relative Angle, °
γ	Gas Expansion Ratio
η_{T-T}	Compressor total-to-total Efficiency
ρ	Density (kg/m^3)
k-ε	Turbulence Model k-Epsilon

Abbreviations

ATM	Automatic Topology Meshing
CFD	Computational Fluid Dynamics
GUI	Graphical User Interface
LE	Leading Edge
TE	Trailing Edge

Received on 27.08.2024
Accepted on 24.09.2024
Published on 27.09.2024

1.0 Introduction

Centrifugal compressor was invented during WWII to supercharge reciprocating engines in early fighter planes. The compressor is used in the aircraft industry for fluid compression, turbocharged engines and gas turbines to deliver high pressure, work over a wide range and maintain constant speed which are great for high pressure applications [1]. The basic mechanism of a centrifugal compressor is to increase the fluid's kinetic energy through a rotating impeller [2]. The impeller acts as the primary component of the centrifugal compressor and plays a significant influence on the performance of the entire compressor. In engineering practice, the fundamentals of fluid mechanics and thermodynamic relations are often used to determine the overall size and the performance of the impeller. In designing turbomachinery, the focus is to achieve optimal efficiency and performance. However, when dealing with low-power input applications, the design must address the challenges that come with using low-power. To achieve this, careful consideration of physical and geometric parameters becomes important for the successful design of small-power turbomachinery.

Computational Fluid Dynamics (CFD) is widely used by turbomachinery engineers to evaluate the performance of the turbomachinery design. CFD is a computational tool used to analyse fluid flow through numerical methods and algorithms. By solving complex mathematical equations that describe fluid behaviour, CFD allows engineers to simulate fluid dynamics and get insights into critical parameters like pressure and temperature. This is used in many fields like weather prediction and aerospace engineering to study and optimize fluid flow [3].

The CFD analysis plays a significant role in evaluating the compressor performance. Studies show that detailed CFD analysis and simulation can greatly improve the performance of these compressors especially in niche applications like micro gas turbines [4]. The complexity of designing and optimizing centrifugal compressors proves the potential of CFD to improve performance characteristics [5], with research highlighting the effect of geometrical parameters on compressor efficiency. For example, computational studies of turbocharger compressor diffusers have shown the importance of diffuser design on overall compressor efficiency [6] [7].

This study aims to analyse the physical dimensions of centrifugal compressors and their performance under off-design conditions using CFD. The hypothesis is that CFD using the k-ε turbulence model in Ansys CFX can model the compressor map and give useful insights to the performance characteristics. The study will focus on generating detailed meshing models of the compressor, setting up precisely the boundary conditions in CFD simulations and defining the compressor characteristics in this study. The objectives are to develop a full meshing model, set up the boundary conditions for accurate simulations and test the compressor performance under different operating conditions.

2.0 Methodology

There are a few stages of the process during the project. Each stage must be done precisely to avoid any implications after reaching a certain stage because each stage is related to the other. The methodology of this study consists of Geometry Generation (BladeGen), Mesh Generation (TurboGrid), Pre–Processing (Pre—CFX), Post-Processing (CFD – Post) and ends with Data Extraction where the results will be obtained at this stage.

2.1 Geometry Generation with ANSYS BladeGen

The compressor impeller blade profile was created in the first stage using ANSYS BladeGen as the modeller and the design specifications measurement. Select "Radial Impeller" as the type of blade to use when beginning a new blade design. As shown in Figure 1, the hub and shroud geometry of the blade profile will be the input of the meridional form coordinates. The hub and shroud dimensions are first specified in coordinates in the geometry definition. The hub radius is set to (r_{1h}) 3.9mm and the shroud radius is set to (r_{1s}) 10mm. These values establish the inner and outer boundaries of the blade. Furthermore, the blade geometry is created by setting the outlet radius to (r_2) 19mm and outlet length of (b_2) 4.1mm. The trailing edge (TE) height is 70mm and the leading edge (LE) thickness is set to 1mm with 12 numbers of blades. Furthermore, it involves 10 blades in total for the impeller design. These variables are essential for establishing the blade's primary geometrical characteristics. As demonstrated in Figure 2, BladeGen graphical user interface is used to view and fine-tune the blade shape, making sure that the hub and shroud transition smoothly.

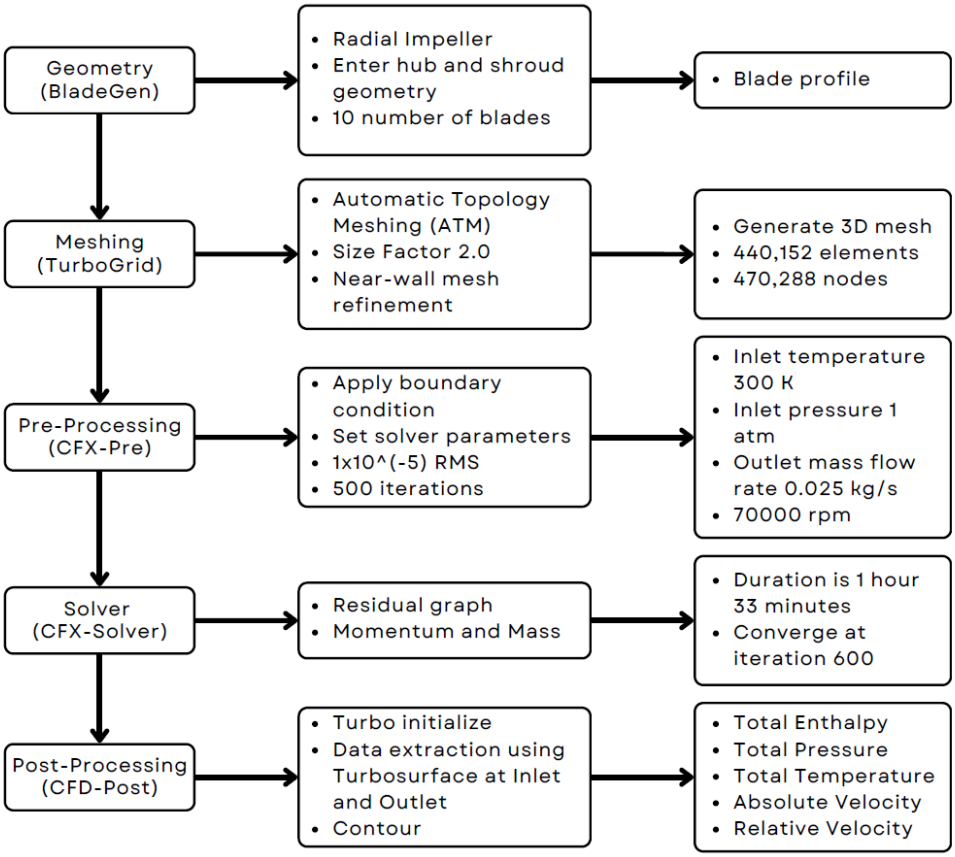

Figure 1: Flow chart of methodology

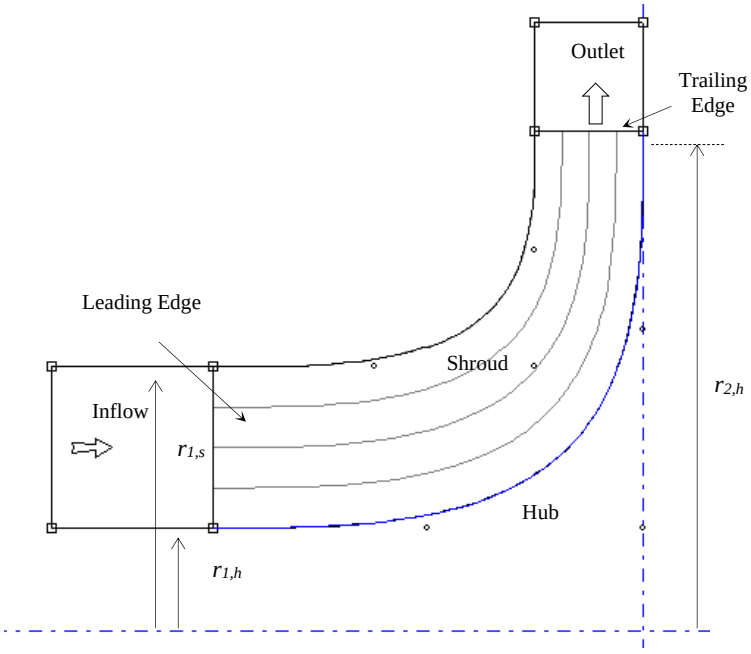

Figure 2: Meridional shape of the blade

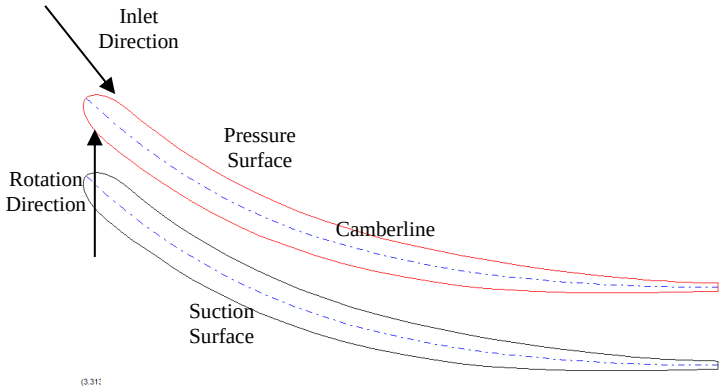

Figure 3: Blade profile modeller

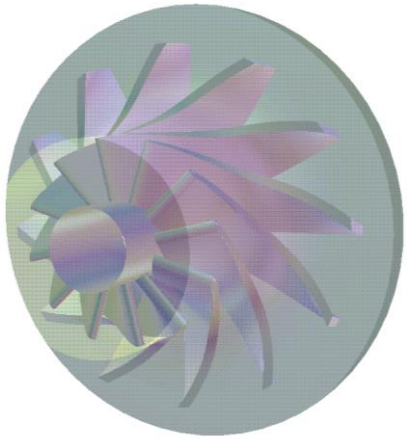

Figure 4: 3D view of the impeller

2.2 Mesh Generation with ANSYS TurboGrid

In computational fluid dynamics (CFD) simulations of centrifugal compressors, generating a high-quality mesh is crucial to accurately capture the flow behaviour [8]. The mesh generation process begins by importing the blade geometry from ANSYS BladeGen into ANSYS TurboGrid. Here, the Automatic Topology Meshing (ATM) technique is employed to automate the identification of critical regions and blade passages within the complex geometry. The entire mesh generating process is simplified by this automation, which significantly decreases user interaction [9].

Table 1 shows the meshing parameter setup for a single passage impeller. The overall element size is determined by consistently applying a global size factor of 2.0 throughout the computing domain. This factor is an attempt to strike a fair balance between mesh resolution and computing efficiency. The bigger size factor produces a finer mesh essential for capturing more accurate flow details, but it also uses more processing power. Boundary layer refinement is turned on to guarantee proper mesh resolution in boundary layers, which is essential for precisely capturing viscous effects close to walls. By increasing the element count in boundary layers proportionately to the global size factor, this refinement produces a finer mesh near walls while preserving an effective overall mesh structure. To guarantee a uniform element size distribution, the element distribution is maintained proportional to the spanwise direction.

To guarantee a highly fine mesh in boundary layers, the absolute sizing is used in near-wall mesh generation, regardless of the global size factor. This method specifies a particular element size close to walls. After defining these settings, ANSYS TurboGrid creates the final 3D mesh. The goal of this mesh setup is to keep computational efficiency while collecting fine-grained flow information. The meshing that has been generated consists of 446886 nodes and 417312 elements, offering a strong basis for ensuing CFD studies of the flow characteristics and performance of the centrifugal compressor. Figure 5 shows the generated meshing for the single impeller.

Table 1: General meshing parameter for TurboGrid

Parameter	Method
Topology Mesh Technique	ATM
Size Factor	2.0
Boundary Layers Refinement Control	Proportional to Mesh Size
Spanwise Blade Distribution Parameter	Proportional
Hub Tip Mesh Method	Match Expansion at Blade Tip
Near Wall Treatment	Absolute

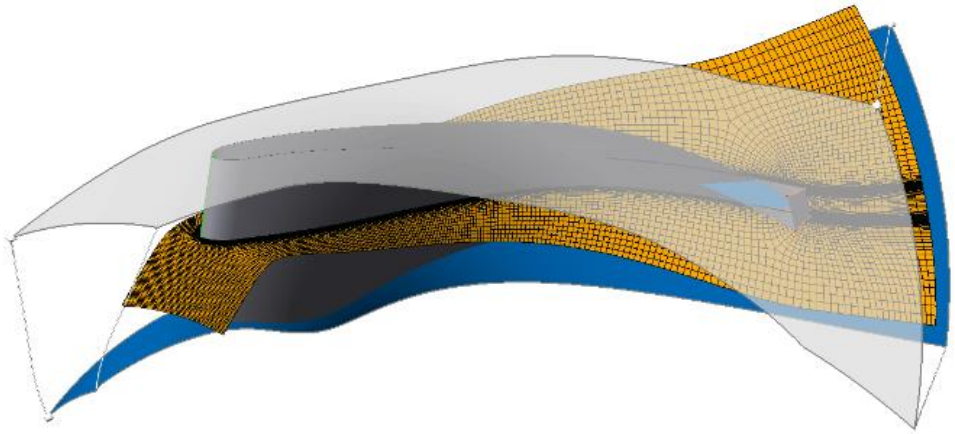

Figure 5: Single impeller passage mesh

2.3 Pre-Processing (CFX-Pre)

CFX-Pre is part of the tools used within ANSYS to complete the pre-processing phase of the CFD simulation. This step will set up the analysis condition, define fluid physical characteristics, and enforce the boundary conditions, which are claimed to accurately capture the operation of a centrifugal compressor [10]. First, import the ANSYS TurboGrid mesh into CFX-Pre. The quality of the mesh is checked once it is imported to ensure it is good enough for an accurate CFD simulation. This step involves searching for any distorted or skewed elements which may affect the results of the simulation.

Fluid properties are then defined within CFX-Pre. The working fluid is specified air as an ideal gas. To ensure that the simulated operating parameters properly define the centrifugal compressor, the density and viscosity of air are set at standard atmospheric conditions. The boundary conditions as shown in Table 2 are applied to the simulation model in the CFX-Pre. Having the flow direction normal to the boundary, at the inlet boundary, the static temperature is set at 300 K with a static pressure of 1 atm. The operating flow rate of the compressor is decided by the mass flow rate per passage, which varies from 0.001kg/s to 0.007kg/s as the off-design conditions, considering the design mass flow rate of 0.0025 kg/s. The strength and predictability of this k-ε turbulence model make it suitable in a lot of industrial applications. As this k-ε turbulence model represents reasonable strength, reliability and predictability, this turbulence model is selected to simulate the turbulent flow behaviour.

In CFX-Pre, the impeller rotational motion is simulated using a technique that incorporates a rotating reference frame. This method accurately models the relative motion between the impeller and stationary components such as the diffuser and volute [9]. Following this setup, solver control parameters are adjusted as outlined in Table 3. High-resolution turbulence settings are implemented to capture complex turbulent flow patterns effectively. To ensure convergence of the solution, the simulation is set to run for a total of 600 iterations. Convergence criteria are defined using RMS (root mean square) residuals, with a target value of 1×10-5. These steps are crucial in achieving highly precise simulation results.

Once all the initial setup steps are completed in CFX-Pre, the configuration is saved and prepared for the next phase in ANSYS CFX. Thorough preparation of the simulation conditions ensures an accurate representation of the operational and physical traits of the centrifugal compressor. This careful setup lays the foundation for obtaining reliable and precise simulation outcomes.

Table 2: Boundary Conditions

Parameter	Values
Speed	60,000rpm, 70,000rpm, 80,000 rpm
Fluid Type	Air Ideal Gas
Turbulence Model	k-ε
Inlet Static Pressure	1 atm
Inlet Static Temperature	300 K
Flow Direction	Normal to Boundary
Mass Flow Type	Per Passage
Mass Flow Rate for 12 blades	0.01 kg/s - 0.065 kg/s

Table 3: Solver Control Setup

Parameter	Values
Turbulence Numerics	High Resolution
Iterations	500
Convergence Criteria	RMS
Residual Target	1 x 10^5

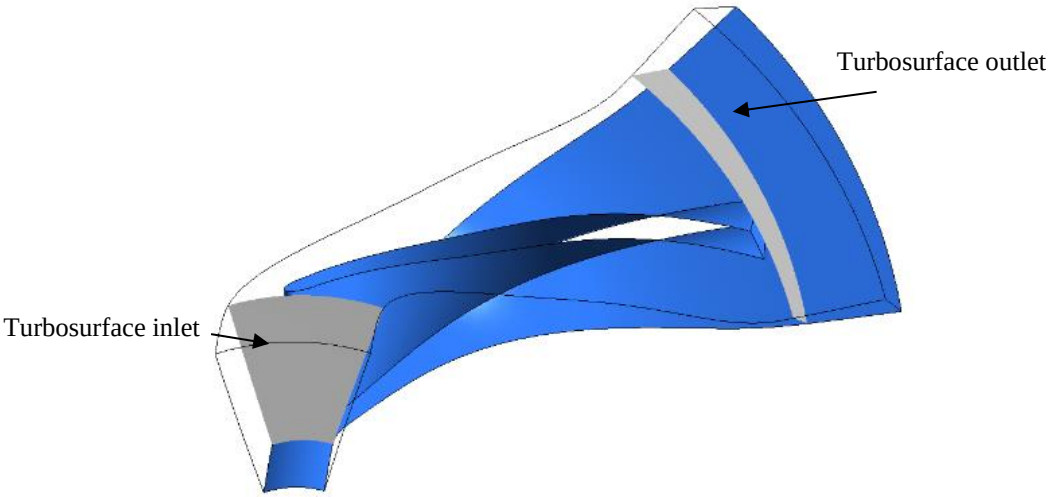

Figure 6: Position of turbosurfaces at inlet and outlet regions

2.4 Post-Processing Methodology Using CFD-Post

The “massflowAve” function is used during the CFD-Post post-processing stage of the simulation to extract the main flow parameters from turbosurfaces that are placed strategically in the inlet and outlet regions near to the compressor blades. These turbosurfaces are needed for data extraction to provide comprehensive information on the flow characteristics at critical points in the centrifugal compressor.

The configuration of turbosurfaces in the inlet and outlet areas is illustrated in Figure 6, which indicates the optimal positioning immediately preceding the flow’s entrance to and exit from the compressor impeller. The "massflowAve" function ascertains the mass-averaged value of a specified parameter over the turbosurface area to derive the relevant information. The formulation for "massflowAve" is given in Equation (1).

$$mass\ flow\ Ave = \frac{\sum y_i \dot{m}_i}{\dot{m}_i} \quad (1)$$

The step involves extracting key parameters such as relative velocity, total temperature, total pressure, total enthalpy, and stationary frame velocity from the turbosurfaces at both the inlet and outlet of the compressor. A detailed analysis of this data is conducted to evaluate various aspects of the compressor's performance. By comparing total pressure and temperature between the inlet and outlet, the study examines how pressure rises, and heat are managed within the compressor. Total enthalpy data provide insights into energy transformation within the flow, while velocity measurements help to detect potential issues like flow separations and provide a clearer picture of flow dynamics.

The data being extracted are also used to develop the centrifugal compressor performance map that determines the performance of the compressor by different operating conditions. The data from the CFD analysis are used by the following parameter:

Pressure Ratio, $PR = \frac{P_{02}}{P_{01}}$ (2)

Corrected Mass Flow Parameter, $\dot{Q}_{corr} = \dot{m}\left(\sqrt{\frac{T_{ref}}{T_{02}}}\right)\left(\frac{P_{02}}{P_{ref}}\right)$ (3)

Compressor Actual Power Input, $\dot{W}_{C,a} = \dot{m}(U_2 C_{\theta 2} - U_1 C_{\theta 1})$ (4)

Compressor Isentropic Power, $\dot{W}_{C,is} = \dot{m} C_p (T_{02s} - T_{01})$ (5)

Compressor Efficiency, $\eta_{T-T} = \frac{\dot{W}_{C,is}}{\dot{W}_{C,a}}$ (6)

In developing the performance map, the corrected mass flow rate is used to plot the map by using Equation (3). The mass flow rate is corrected to 298 K and 101325 Pa; it is to standardise the performance data across different operating conditions instead of actual mass flow [11]. This correction accounts for variations in inlet temperature and pressure, ensuring that the mass flow rate is referred to as a common set of conditions which is sea level standard day.

The flow field analysis is conducted at the design point to synthesise the flow phenomenon in the flow. This post-processing method ensures accurate capture and understanding of all critical flow data. Insights collected from turbosurface data offer a comprehensive view of the compressor's operational behaviour under simulated conditions. These findings are valuable for optimizing the compressor's performance and design, aiming for reliable and efficient operation in practical applications.

Table 4: Velocity Triangle and at the Design Point

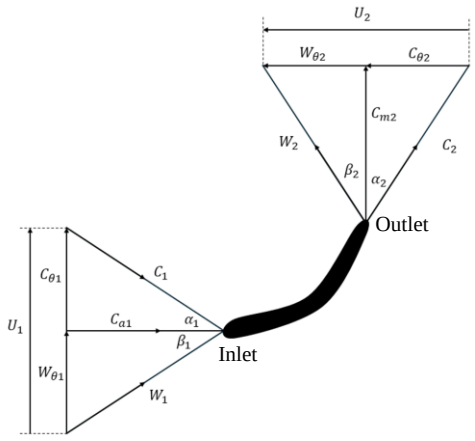

Inlet Velocity Components	Inlet (1)	Outlet (2)
Meridional Velocity, C_m	79.2 m/s	43.1 m/s
Blade Velocity, U	73.3 m/s	139.3 m/s
Absolute Velocity, C	79.2 m/s	142.1 m/s
Relative Velocity, W	107.9 m/s	43.3 m/s
Rel. Tangential Velocity, W_θ	73.3 m/s	-3.9 m/s
Tangential Velocity, C_θ	0 m/s	135.4 m/s
Relative Angle, β	-42.9°	-5.1°
Absolute Angle, α	0.0°	72.3°
Total Enthalpy, h_0	1037.9 kJ/kg	20211.4 kJ/kg
Total Pressure, P_0	103920 Pa	146018 Pa
Total Tempretature, T_0	299.2 K	318.3 K

3.0 Result and Discussion

Initially the compressor is analysed at the design point which is at the mass flow rate of 25 g/s and the turbine rotation speed of 70,000 rpm. Table 4 shows the velocity triangle for the compressor and the respective values for the velocity triangle components. The data are extracted at the turbosurface of the inlet and outlet. At the inlet, the fluid has an enthalpy value of 1037.9 J/kg, total pressure of 103,920 Pa, and a total temperature of 299.2 K. Its absolute velocity is 79.2 m/s, and the relative velocity is 73.3 m/s. The absolute angle, α_1 and the relative angle, β_1 is 0° and -42.9°, respectively. This indicates that the flow enters at axial direction. The total enthalpy at the outlet significantly increases to 202111.4 kJ/kg with the total pressure of 146018 Pa. These values significantly rise to 20211.4 J/kg of enthalpy at the outlet, while total pressure increases to 146,018 Pa and the total temperature increases to 318.3 K. To add, the absolute velocity at the outlet increases to 142.1 m/s while relative velocity decreases to 41.5 m/s. The absolute angle at the inlet, α_2 is 72.3° and the relative angle, β_2 is -5.1°. These suggest a highly intensive energy addendum and transformation in the compressor.

During the compression process, mechanical energy is changed into fluid energy; thus, there will be a rise in temperature, enthalpy, and total pressure from the inlet to the outlet. A large amount of kinetic energy gets to be added to the fluid in this process, which is observed by the increase in absolute velocity. Since the reference is changed by interaction with the rotating impeller, there will be a decrease in relative velocity. Those variations must be understood for better optimization of compressor efficiency, localization of areas of high energy input, and identification of possible losses. Further analyses and modelling give insight into enhancing performance and efficiency in centrifugal compressors.

3.1 Performance Map

Figure 7 shows the relationship between the pressure ratio and the mass flow rate at three different rotational speed which are 60,000 rpm, 70,000 rpm, and 80,000 rpm as shown in the centrifugal compressor performance map. This parameter demonstrates the operating conditions of the centrifugal compressor. As the mass flow rate increases for each speed, the pressure ratio first climbs to a peak value and then falls. The compressor obtains the largest pressure ratios at 80,000 rpm, which ends at around 1.534 at about 0.038 kg/s. At the highest corrected mass flow rate of 0.083 kg/s, the compressor decreases even more dramatically to about 1.176. At around 0.035 kg/s, the 70,000 rpm curve displays the highest peak pressure ratio of 1.405, which steadily declines to 1.094 at the maximum mass flow rate. At a corrected mass flow rate of around 0.026 kg/s, the 60,000 rpm curve shows the largest pressure ratio of 1.291, which progressively decreases to about 1.013 as the mass flow rate just before the choke point. In general, as the mass flow rate increases, greater rotational speeds lead to larger pressure ratios but also a more noticeable reduction in pressure ratio. The map shows the compressor choke point which is at 0.065 kg/s for all rotational speed, and the compressor ability to maintain at the large pressure ratio is compromised, leading to a significant drop in efficiency as shown in Figure 8. Figure 8 shows the compressor efficiency with different rotational speed. The plotted graph shows that the efficiency of the centrifugal compressor decreases when the pressure ratio is increased.

3.2 Impeller Aerodynamic Flow field

The centrifugal compressor's fluid speed changes are shown by the stationary frame contours' velocity. Centrifugal force causes the fluid to speed up as it moves from the hub to the shroud. The maximum speeds are observed in the vicinity of the blade tips, suggesting that the fluid and the blades are effectively transferring energy. Notable slowdowns close to the hub, however, may indicate areas of uneven flow and potential flow separation that lead to inefficiencies. These differences aid in pointing out potential locations for design enhancements to better control the flow.

In order to further analyse the effect of the flow field, the passage is divided into five (5) cross sections, and the absolute velocity, *C* and the static entropy, *s* are analysed. Figure 9 shows the meridional view of the cross section. The passage is cut at the span ratio of 0.23, 0.365, 0.55, 0.635 and 0.77 from the boundary inlet to the boundary outlet. At the 0.23 span, the cross section is located before the LE and at the cross section at the span of 0.77 is located after the LE. The location is properly selected to avoid the chaotic flow near to the LE and TE.

In the flow filed analysis, the absolute velocity is selected because the main loss of the friction loss is highly contributed by the absolute velocity [12]. The difference of the absolute velocity in the flow passage generates vorticity or the curl of the flow and generates the passage loss in the compressor passage. The compressor's energy loss regions are shown by the static entropy contours. Figure 10(a) and Figure 10(b) depict five cross sections over the span of the passage for the contour of velocity in Stationary Frame or absolute velocity, *C* contour and the static entropy contour, respectively. At the inlet (span = 0.23), a high velocity is observed near to the shroud

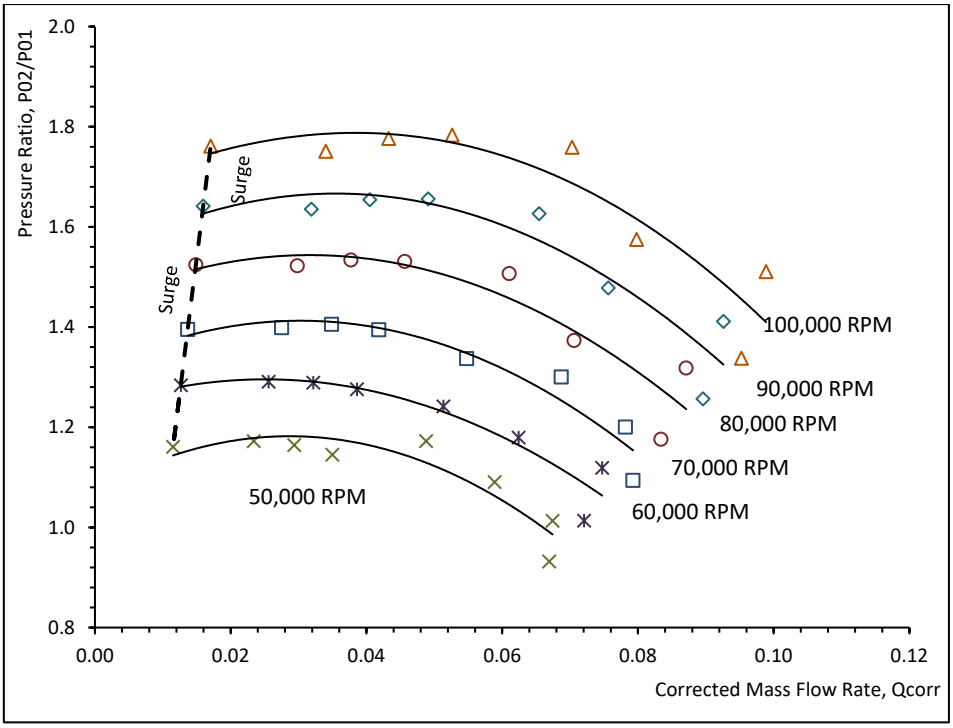

Figure 7: Compressor Performance Map

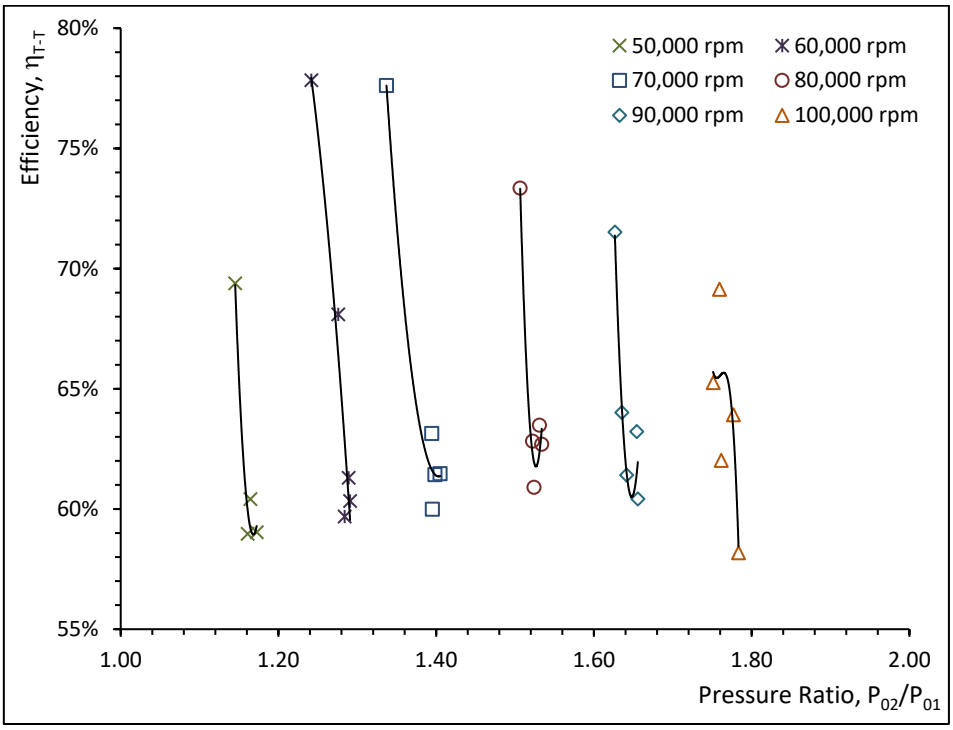

Figure 8: Efficiency against Pressure ratio

region and low velocity region is located at the upper section of the LE. The effect of the velocity change can be observed in the static entropy contour where a higher entropy is generated near the shroud section. The high velocity region is also observed at the span of 0.365 and a variation of velocity changes is observed near the Pressure Surface (PS). Thus, the entropy is significantly generated near the PS area. Similar trend is also observed at the span of 0.5 and 0.635 where higher velocity changes happen near the PS and generate a large entropy in that area. In addition, the effect of the tip clearance which is the distance between the impeller tip and the shroud can be clearly observed at the span of 0.5 and 0.635 where a higher velocity is observed in this region. At the final cross section (span = 0.77), it shows a higher absolute velocity near the TE of the impeller and subsequently generates a large static entropy in that region.

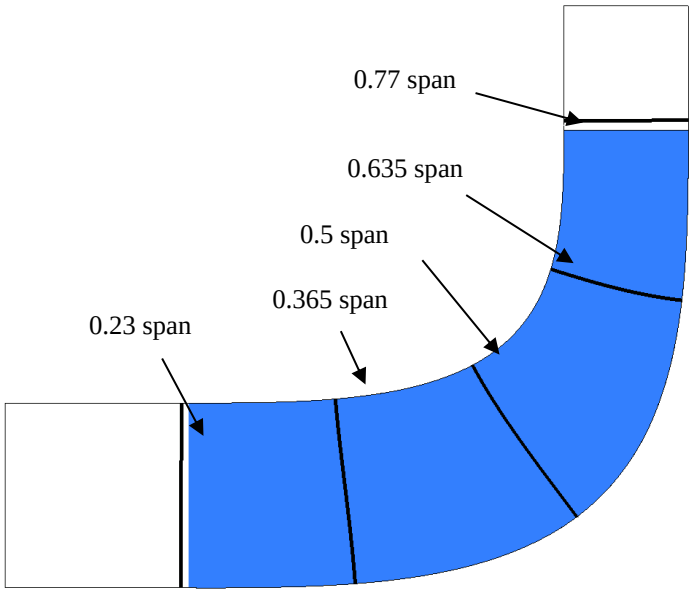

Figure 9: Span position for impeller aerodynamic flow field

(a) Velocity in Stn Contour

(b) Static Entropy Contour

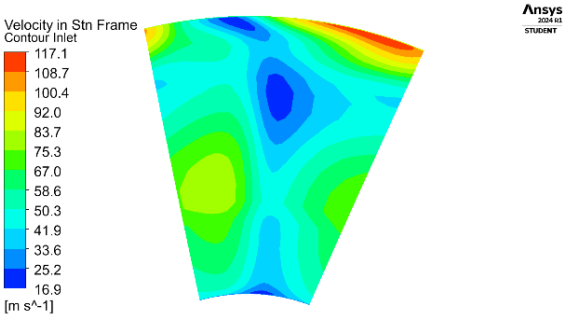

(i) 0.23 span

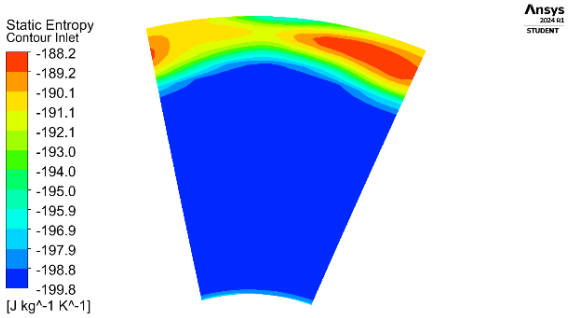

(i) 0.23 span

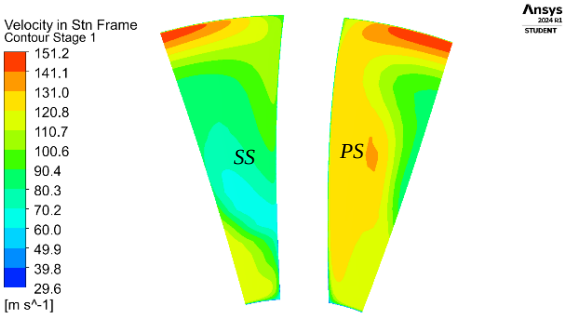

(ii) 0.365 span

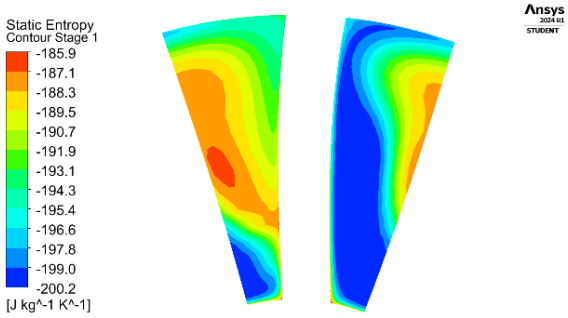

(ii) 0.365 span

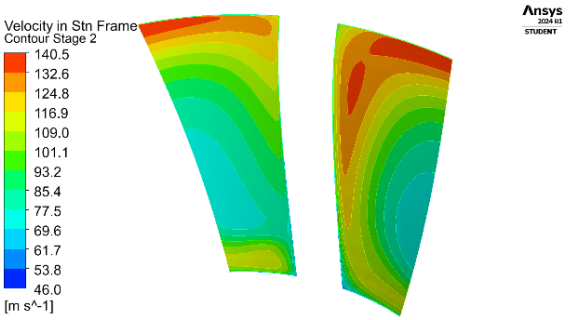

(iii) 0.5 span

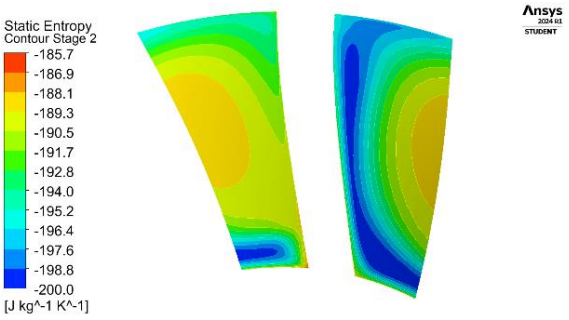

(iii) 0.5 span

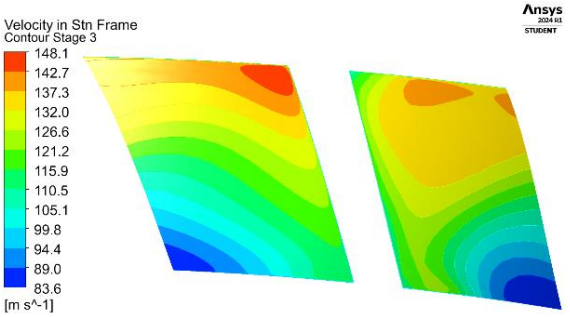

(iv) 0.635 span

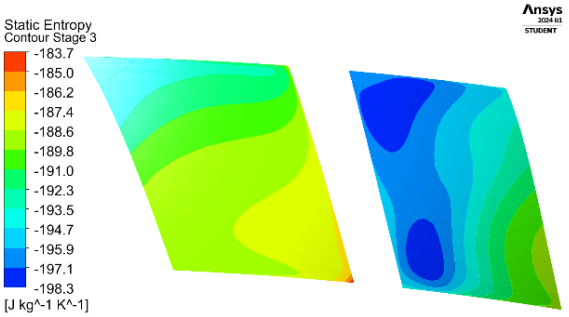

(iv) 0.635 span

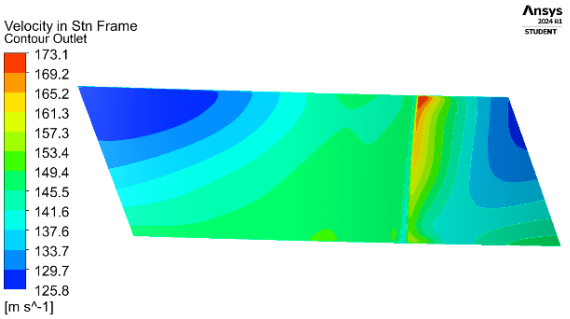

(v) 0.77 span

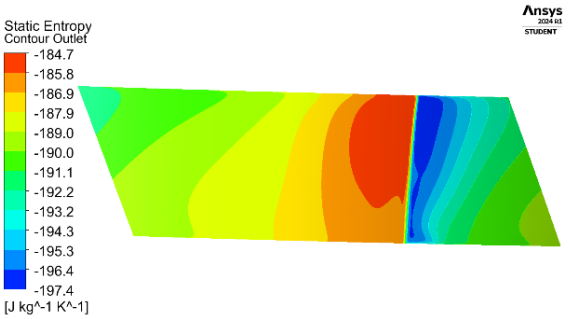

(v) 0.77 span

Figure 10(a): Velocity contour

Figure 10(b): Static entropy contour

3.3 Pressure Blade Loading

Figure 11 shows the positions of the span for pressure blade loading which are 0.1 span at the hub region, 0.5 span at the middle of the blade and 0.9 span at the shroud region. This shows the pressure distribution along the blade span where the amount of pressure changes along the blade chord from the leading edge to the trailing edge.

Figure 12 illustrates the total pressure in stationary frame against the streamwise coordinates (0 to 1) of the centrifugal compressor blade span. At the 0. 1 span hub region, it is situated near the bottom and close to the axis of rotation of the blade, the pressure is small and gradually rises with the increase of the length of the blade. The 0.5 span at middle of the blade is located halfway between hub and shroud, which depicted higher pressure values and proving that there is better energy transfer. The 0.9 span shroud region at the top of the blade near the outer edge has the highest total pressure, which confirms that there is energy addition and higher aerodynamic load in this region. The pressure loading profiles have facilitated the differing span positions of the blade loading at the different zones of the impeller span which gives a significant impact due to the distribution of the aerodynamic forces from the hub region to the shroud region. A large pressure distribution difference between the PS and SS generates a larger area under the graph. Thus, the impeller torque is increased as the area under the Total Pressure, P0 is against the Streamwise direction. If the area is larger at the shroud area (higher span ratio), the impeller loading is large at that region and might cause a structural failure due to the flutter and vibration. This situation might happen at the surge and choke region (refer to Figure 7).

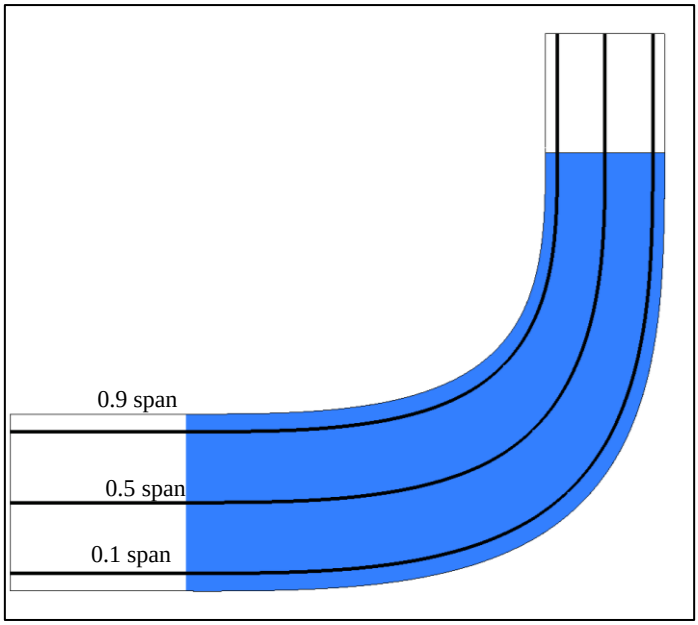

Figure 11: Meridional view of the span position

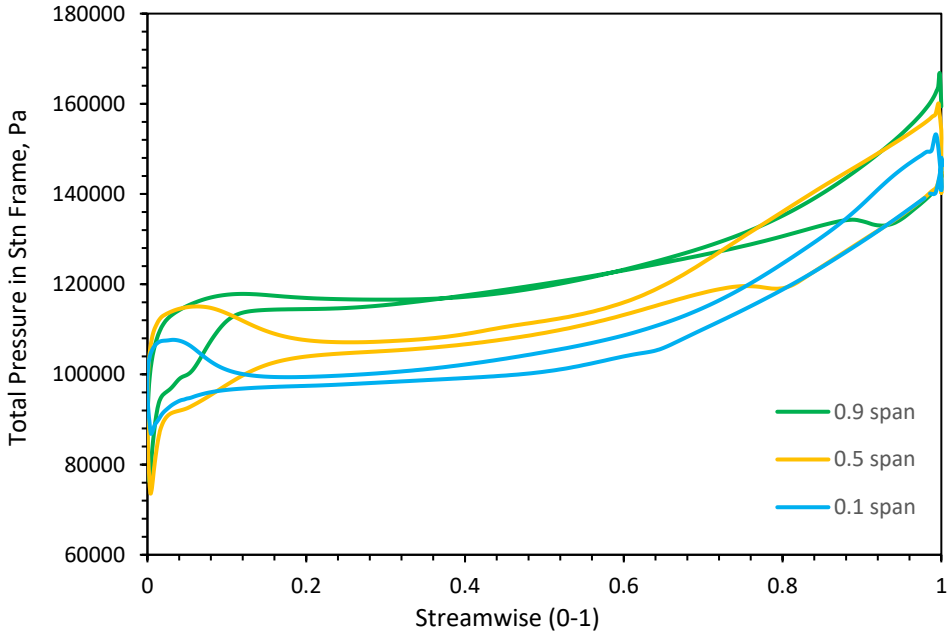

Figure 12: Pressure blade loading from hub to shroud area

4.0 Conclusion

The objectives of the study are to analyse and improve the performance of a 500W centrifugal compressor using computational fluid dynamics; thus, the objectives are met. An in-depth study was devoted to finding the key variables at three different rotational velocities of 60,000, 70,000, and 80,000 rpm. The variables under investigation were mass flow rate, pressure ratio, and efficiency.

It is observed that, with an increase in mass flow rate, the pressure ratio increased to a high value before it started falling. The highest pressure ratio was recorded at 100,000 rpm, whereby the peak of the pressure ratio was about 1.80. Pressure ratio decreased noticeably with the maximum mass flows, indicating the choke point of the compressor, which was around 0.1 kg/s for all rotational speeds. This underlines the importance of optimizing compressor design and operation characteristics to enhance efficiency and the compressor capacity.

The analysis has also come up with a huge amount of energy addition and conversion within the centrifugal compressor. Considerable changes in temperature, velocity, pressure, and enthalpy have been discovered between the input and outflow at 70,000 rpm. The total pressure increased from 104,217 to 147,937 Pa, and the temperature

increased from 299.3 K to 318.5 K. The enthalpy increased from 1173.4 J/kg at the inlet to 20,462.6 J/kg at the outflow. The relative velocity dropped, however, to 39.2, while the absolute velocity remained at the value of 143.0 m/s at the outlet. Those changes indicate that a lot of energy addition and transformation has taken place within the compressor.

The performance map indicates the operating boundaries and the efficiency of the compressor. Presented herein are the results showing the best operating conditions of the compressor and how different rotational speed affects its efficiency. The set goals in this study are finally met because this work enunciated the performance characteristics of the centrifugal compressor, hence bringing out areas that are of most need for further improvement.

In summary, the study provides some insightful information to be used in guiding further centrifugal compressor design and operating tactics by using a single passage impeller CFD simulation. Knowledge from the study provided the basis necessary for increasing these compressors' accuracy and effectiveness. The more serious approaches of research and modelling that would deal with the areas of significant energy loss, especially at the blade tips and mid-span, may be required by increasing the efficacy of compression and higher overall efficiency. Other factors that can improve compressor performance involve new blade designs and material properties.

References

[1] H. I. H. Saravanamuttoo, G. F. C. Rogers, and H. Cohen, "Gas Turbine Theory (5th Ed.)," *Gas Turbine Theory (5th Ed.)*, 2001.

[2] V. V Kulkarni, T. R. Anil, and N. K. S. Rajan, "An Impeller Blade Analysis of Centrifugal Gas Compressor Using CFD," *International Journal of Innovations in Engineering and Technology (IJIET)*, vol. 217, no. 4, 2016.

[3] T. Barza and G. Lakshmikanth, "Flow Simulation And Performance Analysis Of Centrifugal Compressor Using Cfd_Tool," *Journal of University of Shanghai for Science and Technology*, vol. 23, no. 11, 2021.

[4] R. Aghaei tog, A. Mesgharpoor Tousi, and M. Soltani, "Design and CFD analysis of centrifugal compressor for a microgasturbine," *Aircraft Engineering and Aerospace Technology*, vol. 79, no. 2, pp. 137–143, Jan. 2007, doi: 10.1108/00022660710732680.

[5] B. Mostefa, R. Kaddour, D. Embarek, and K. Amar, "Analysis and optimization of the performances of the centrifugal compressor using the CFD," *International Journal of Heat and Technology*, vol. 39, no. 1, 2021, doi: 10.18280/ijht.390111.

[6] J. Galindo, A. Gil, R. Navarro, and D. Tarí, "Analysis of the impact of the geometry on the performance of an automotive centrifugal compressor using CFD simulations," *Appl Therm Eng*, vol. 148, pp. 1324–1333, Feb. 2019, doi: 10.1016/j.applthermaleng.2018.12.018.

[7] B. S. Gopi and P. S, "Design and Computational Analysis of the Conventional Vaned Diffuser for a Turbocharger Compressor," *Int J Res Appl Sci Eng Technol*, vol. 11, no. 1, pp. 1026–1031, Jan. 2023, doi: 10.22214/ijraset.2023.48757.

[8] M. Omidi, S. J. Liu, S. Mohtaram, H. T. Lu, and H. C. Zhang, "Improving centrifugal compressor performance by optimizing the design of impellers using genetic algorithm and computational fluid dynamics methods," *Sustainability (Switzerland)*, vol. 11, no. 19, 2019, doi: 10.3390/su11195409.

[9] Inc. ANSYS, "Ansys TurboGrid User's Guide." Accessed: Jun. 11, 2024. [Online]. Available: https://www.ansys.com/products/fluids/ansys-turbogrid

[10] A. Eza, "Flow simulations with relevance to a centrifugal compressor and the e ect of the inlet geometry," *Master thesis*, 2015.

[11] G. F. C. Rogers and Y. R. Mayhew, "Engineering thermodynamics work and heat transfer: SI units. 3rd ed.," 1980.

[12] Japikse, D. and Baines, N. C., *Introduction to Turbomachinery*, First ed., Concepts ETI Inc; Oxford University Press, Vermont, 05055, USA, 1994.